International Journal of Remote Sensing
Vol. 34, No. 6, 20 March 2013, 1995–2005

Taylor & Francis
Taylor & Francis Group

In-flight absolute calibration of an airborne wide-view multispectral imager using a reflectance-based method and its validation

Wei Chen[a,b,c,d], Lei Yan[a,c,d], Zhanqing Li[b]*, Xin Jing[a,c,d], Yini Duan[a,c,d], and Xiaoxiong Xiong[e]

[a]*School of Earth and Space Science, Peking University, Beijing 100871, PR China;* [b]*Earth System Science Interdisciplinary Center, University of Maryland, College Park, MD 20740, USA;* [c]*Institute of RS & GIS, Peking University, Beijing 100871, PR China;* [d]*Beijing Key Lab of Spatial Information Integration and its Applications, Peking University, Beijing 100871, PR China;* [e]*NASA Goddard Space Flight Center, Code 618, Biospheric Sciences Laboratory, Greenbelt, MD 20771, USA*

(*Received 19 February 2012; accepted 9 September 2012*)

The wide-view multispectral imager (WVMI) is the main instrument carried on an unmanned vehicle in the Unmanned Vehicle Payloads Comprehensive Calibration Campaign, which focuses on the calibration and validation of various remote-sensing sensors, including multispectral and hyperspectral sensors. In order to calibrate the WVMI, we designed and deployed a set of six radiometric calibration targets with nominal reflectances of 4%, 20%, 30%, 40%, 50%, and 60% and a set of four radiometric validation targets, the reflectance spectra of which vary dramatically with wavelength. The results reveal a good linear relationship between the digital number (DN) of each sensor and the apparent radiances. Further analysis of data from the validation targets reveals that both spectral unevenness and low reflectance will lead to incurrence of errors in calculations using the calibration equation. This suggests a potential problem that needs to be addressed in the remote sensing of vegetation.

1. Introduction

In-flight absolute calibration plays an increasingly important role in remote-sensing applications by connecting the response output of a sensor with the real energy it receives (Slater et al. 1987; Gao et al. 2010). Research over the past decades has shown overwhelmingly that the accuracy of the absolute calibration of a remote-sensing imager will affect the quality of the retrieval of biophysical and geophysical parameters of the land surface as well as of the atmosphere (Thome 2001; Biggar, Thome, and Wisniewski 2003; Xiong and Barnes 2006; Cihlar, Chen, and Li 1997; Lee et al. 2009; Li et al. 2009; Gao et al. 2010; Naughton et al. 2011). Radiometric calibration is the first step in any remote-sensing application. It is also the precondition for the synergy of multisource data assimilation.

In-flight absolute calibration methods rely on *in situ* measurements of the ground reflectance and atmospheric parameters (Biggar et al. 1991). There are three basic in-flight absolute calibration methods for remote-sensing instruments (Slater et al. 1987; Biggar,

*Corresponding author. Email: zli@atmos.umd.edu. Present address: State Key Laboratory of Earth Surface Processes and Resource Ecology, GCESS, Beijing Normal University, Beijing 100875, China.

ISSN 0143-1161 print/ISSN 1366-5901 online

http://dx.doi.org/10.1080/01431161.2012.730160
http://www.tandfonline.com

Santer, and Slater 1990; Biggar et al. 1991): the reflectance-based method, the irradiance-based method, and the radiance-based method. The reflectance-based method is the most convenient approach with a relatively higher uncertainty than that from the other two approaches. However, its uncertainty still falls within a reasonable range (Biggar, Slater, and Gellman 1994). Recent research reveals that the uncertainty of the reflectance-based method can reach 2.5% (Thome 2005; Naughton et al. 2011). The reflectance-based method has been widely employed for both airborne and spaceborne remote-sensing payloads, such as the Landsat Enhanced Thematic Mapper Plus (ETM+) (Thome et al. 2004), the Système Pour l'Observation de la Terre (SPOT) High Resolution Visible (HRV) (Rondeaux et al. 1998), and the China–Brazil Earth Resources Satellite No. 2 (CBERS-02) visible and infrared bands (Zhang et al. 2005). In this article, we adopt the reflectance-based method as the fundamental calibration approach to correct wide-view multispectral imager (WVMI) data.

Although the radiometric calibration of spaceborne payloads has been widely developed in China, not enough attention has been paid to the in-flight calibration of airborne payloads. Compared to the widely established calibration field sites for satellite instruments, such as the White Sands Missile Range in the USA, La Crau in France, and Dunhuang in China, there are few calibration field sites specifically designed for airborne sensors. This is due to the lack of airports suited to this activity, complicated weather conditions, and the high cost of running such field campaigns. In response to this need, the Unmanned Vehicle Remote Sensing Load Comprehensive Calibration Fields project was proposed and sites were constructed in both Inner Mongolia and Guizhou Province, China. The first calibration campaign, called the Unmanned Vehicle Payloads Comprehensive Calibration Campaign, was carried out on 14 November 2010 in Inner Mongolia. In this article, we use data from this campaign to get a comprehensive understanding of the factors that contribute to errors and uncertainties in radiometric calibration. We describe the method of in-flight absolute radiometric calibration of the WVMI and present results for the bands that were imaged successfully. Potential errors germane to future applications are discussed.

2. Overview of the WVMI

The WVMI is one of two payloads on the unmanned vehicle, which is focused on quantifying the retrieval of surface geophysical parameters. Its sensor is a push-broom charge-coupled device (CCD) with four multispectral bands, ranging from blue to infrared, and one panchromatic band. For the multispectral band, at a flight height of 2.5 km, the WVMI has an instantaneous field of view (IFOV) of about 0.5 m and a field of view (FOV) of 3 km (images contain 6000 pixels). For the panchromatic band, at a flight height of 2.5 km, the WVMI has an IFOV of about 0.25 m and a FOV of 3 km (images contain 12,000 pixels). The instrument is designed and manufactured by the Changchun Institute of Optics, Fine Mechanics and Physics, Chinese Academy of Sciences. Before the campaign, a pre-flight laboratory calibration of the WVMI was carried out to identify the normalized response functions of the four multispectral bands. These functions are shown in Figure 1. The panchromatic band, which was going to be used for mapping purposes, was not calibrated in the laboratory and will not be discussed in this article. Cold weather during the campaign led to the failure of calibration of the blue band. In this article, we mainly discuss calibration results and errors in the green, red, and infrared bands of the WVMI.

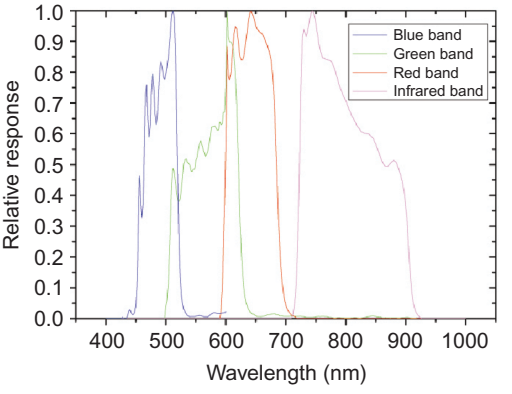

Figure 1. Normalized spectral response functions of the WVMI.

3. Introduction to the calibration field site and calibration targets

3.1. Calibration field site description

The calibration field site is located on flat terrain in a semi-arid region of Inner Mongolia (40° 38′ N, 108° 51′ E). The average altitude of the calibration field site is about 1.2 km and the visibility on clear days is about 70–100 km. The site is located in northern China and borders the Gobi Desert, so there is little rainfall throughout the year. In order to properly calibrate the WVMI, six radiometric calibration targets with nominal reflectances of 4%, 20%, 30%, 40%, 50%, and 60% were designed and produced by Peking University and deployed at the site. The spectral variation of each target is less than 7% in the range of 400–1000 nm, which bodes well for the accurate calibration of the WVMI's spectral bands. Although the real reflectance at each band deviates a little from the nominal value (see Figure 2), this has little effect on the results. In order to validate the calibration results, we also designed four multispectral validation targets whose reflectance spectra are not as

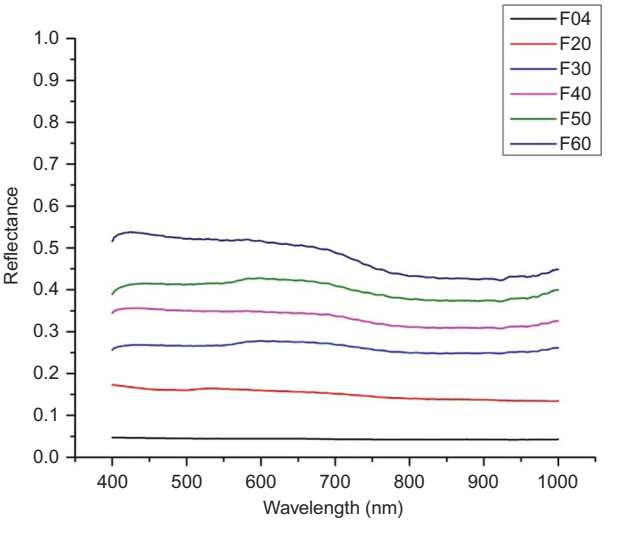

Figure 2. *In situ* measurements of six radiometric calibration targets.

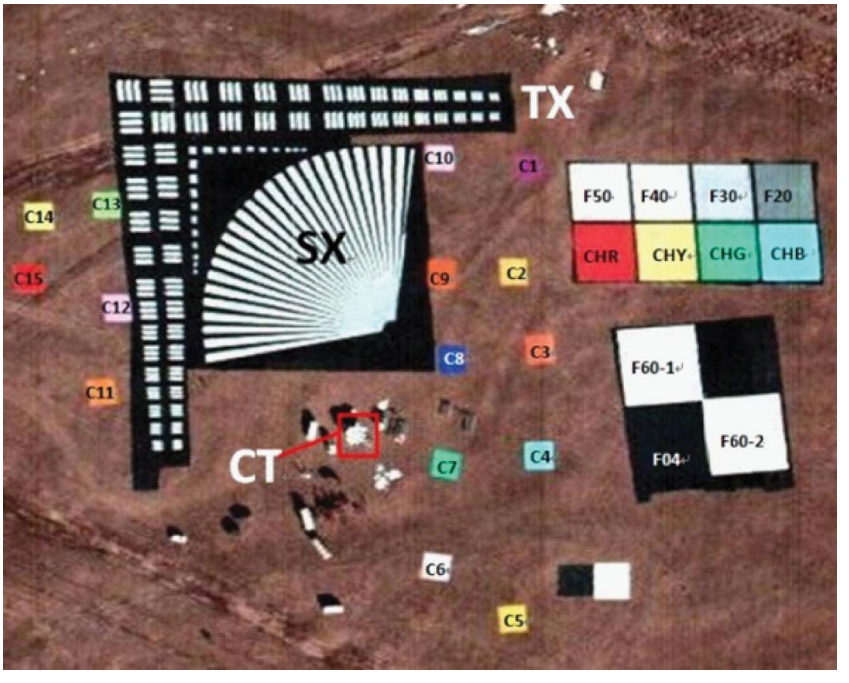

Figure 3. The arrangement of the calibration targets during the campaign.

flat as those of the radiometric calibration targets. A detailed description of the targets is described in Section 3.2.

3.2. Description of the calibration targets

Four kinds of targets are deployed at the site, as shown in Figure 3. The first kind is the set of radiometric calibration targets; these are denoted in the figure as F04, F20, F30, F40, F50, and F60 (split into two, namely F60-1 and F60-2). F indicates the type of target, while the number represents the nominal reflectance of the target. The spectral variation in the range of imaging bands of the WVMI (400–1000 nm) is less than 7%. The F04 and two F60 target sizes are 20 m × 20 m; the target size for F20, F30, F40, and F50 is 15 m × 15 m. The second kind of target is the multispectral evaluation target, denoted as C01–C15 in Figure 3; each target covers 7 m × 7 m. This target is designed to evaluate the performance of the sensors and will not be discussed here. The third kind of target is the multispectral validation target used for validation of the WVMI, denoted as CHR, CHY, CHG, and CHB in Figure 3, and used in this article for estimating the error of calibration brought on by spectral unevenness. Each of these multispectral validation targets covers 20 m × 20 m. The last kind of target is the geometry calibration target used for geometry calibration and correction, denoted as SX, TX, and CT in Figure 3. The results from this type of calibration are also not discussed in this article.

4. Methodology

4.1. Radiometric calibration approaches

The reflectance-based method is the most commonly used approach to calibrate a sensor's visible and near-infrared bands. This approach needs synchronous measurements of surface

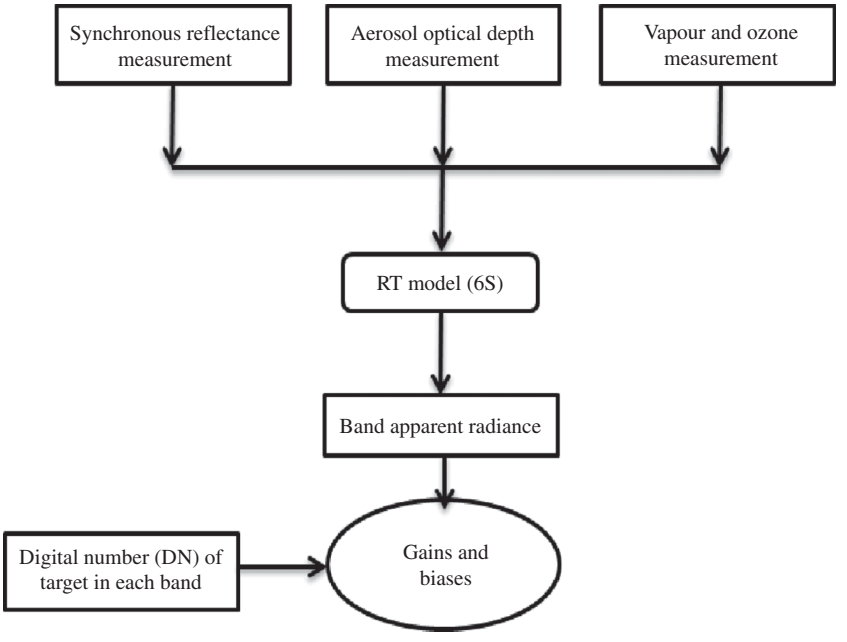

Figure 4. Flow chart of the reflectance-based radiometric calibration.

reflectance, aerosol properties, and meteorological parameters. Reflectance and atmospheric parameters are needed as input into a radiative transfer model, such as Second Simulation of the Satellite Signal in the Solar Spectrum (6S) and Moderate Resolution Atmospheric Transmission (MODTRAN), to calculate the apparent radiance at the top-of-the-atmosphere altitude or at the sensor altitude. The irradiance-based method was a backup method, given that the accuracy of the ratio of diffuse to total radiation is not high. The flow chart describing the reflectance-based method is shown in Figure 4.

4.2. Synchronous measurement of the radiometric calibration targets

During the field campaign dedicated to radiometric calibration on 14 November 2010, the reflectance measurements of the radiometric calibration targets for the WVMI were collected within 1 h before or after the overpass time of the unmanned vehicle. This ensured that synchronous or quasi-synchronous measurements were taken. The slope of the ground for arranging the radiometric calibration targets is less than 3°. Reflectance measurements over each target were collected using a FieldSpec 4 Portable Spectroradiometer manufactured by the ASD with a spectral range of 0.35–2.5 μm; it was set to the radiance mode. We first measured the reference board twice and then randomly collected measurements of the reflectance of each target a minimum of nine times. An additional measurement from the reference board was collected afterwards. Reflectance was calculated by dividing the collected radiances of the targets by the collected radiance of the reference board. Measurements for a single target took less than 3 min to obtain, thus ensuring that the solar zenith angle did not change too much during this time. Aerosol properties were also collected during the campaign. Aerosol optical depths (AODs) were retrieved from measurements collected by a five-channel hand-held Microtops II sunphotometer (Solar

Light Company, Inc., Glenside, PA, USA). Daily AOD at 550 nm varied from 0.03 to 0.09, with an average value of 0.075 during the campaign. This shows that the atmosphere was relatively clear and suitable for performing absolute calibrations of the sensor. NASA's Ozone Monitoring Instrument provided the ozone content.

4.3. Radiative transfer calculations

Models such as 6S and MODTRAN are radiative transfer models commonly used for radiometric calibration. The spectral ranges of the 6S and MODTRAN models are 0.3–4.0 μm and 0.3–100 μm, respectively. The WVMI's spectral range is 0.4–1.0 μm and sampling is done every 2 nm, so running the 6S model at a spectral resolution of 2.5 nm in the visible and infrared spectral range is suitable for the absolute calibration. Apparent reflectance, ρ^*, can be expressed as

$$\rho^* = \frac{\pi L^* d_s^2}{E_0 \cos\theta_s}, \tag{1}$$

where L^* is the apparent radiance the sensor receives, d_s is the Sun–Earth distance factor, E_0 is the irradiance at the top-of-the-atmosphere, and θ_s is the solar zenith angle. Surface reflectance and apparent reflectance have the following relationship:

$$\rho^* = \left\{ \left[\rho_a + \frac{\rho_t}{1 - \rho_t S} T(\theta_s)\, T(\theta_v) \right] \right\} T_g, \tag{2}$$

where ρ_a is the intrinsic reflectance of the atmosphere, ρ_t is the surface reflectance, S is the albedo of the atmosphere, $T(\theta_s)$ is the transmittance between the Sun and the surface, $T(\theta_v)$ is the transmittance between the surface and the sensor, and T_g is the gaseous transmittance. The relationship between surface reflectance and apparent radiance can be established using these two equations.

In our calculations, the solar zenith and azimuth angles at the time of the instrument overpass are 60.47° and 163.37°, respectively. The targets were designed to have Lambertian properties, which are well known, and were positioned at the nadir direction of the sensor, so a Lambertian land surface is assumed in our calculations. These parameters are input to the 6S model and radiances are simulated, representing what the sensor would measure.

5. Results

During the campaign, the blue band failed to capture an image during the flight. As a result, we only calibrated the green, red, and infrared bands. After obtaining the apparent radiance of the ith band, L_i, we selected the central part of each target, covering an area of about 10 × 10 pixels and then calculated the average digital number (DN) for each band. Through the least-squares method, the bias and gain for each band can be obtained using the following calibration equation:

$$L_i = a\mathrm{DN} + b, \tag{3}$$

where a is the gain and b is the bias. Calibration results for each band are shown in Figure 5 (from top to bottom, green, red, and infrared bands). The calibration equations

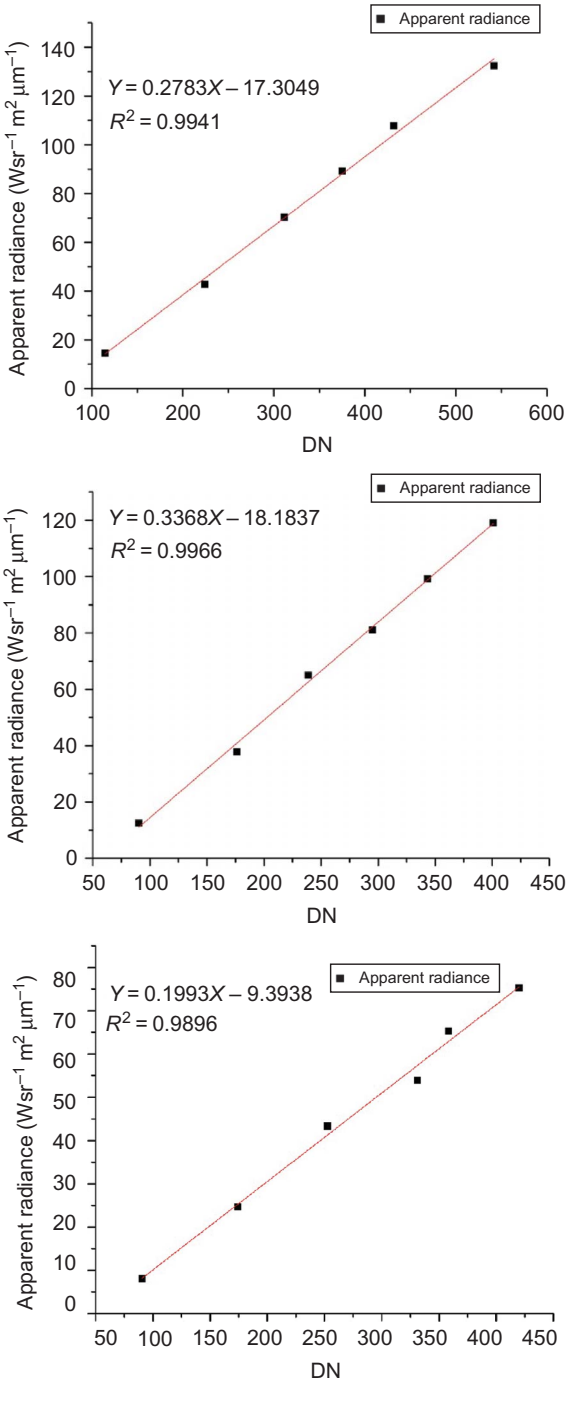

Figure 5. Calibration results of the three multispectral bands (top, green band; central, red band; bottom, infrared band).

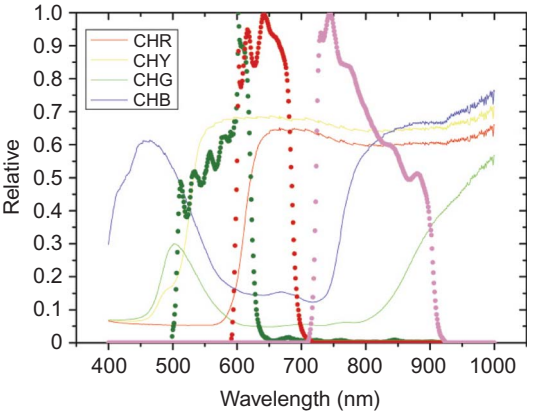

Figure 6. Spectra of the four multispectral validation targets (solid lines) and the spectral response functions of the WVMI's green, red, and infrared bands (dotted lines).

of all three bands are noted in the figure. Correlation coefficients are all of the order of 99%, indicating that the relationship between the sensor response and apparent radiance is linear.

The above results are obtained from radiometric calibration targets with relatively flat reflectance spectra in the range of 0.4–1.0 μm. Over real surfaces, reflectance spectra vary with wavelength. Under these circumstances, the apparent radiance from Equation (3) may differ from radiative transfer calculations.

In order to quantify the error brought on by the spectral variation of reflectance, a set of four multispectral validation targets was designed with different reflectance spectra in the range of 0.4–1.0 μm. Reflectance as a function of wavelength for these targets (solid lines) and the spectral response functions of the WVMI's green, red, and infrared bands (dotted lines) are shown in Figure 6. To mimic reflectance seen in nature, the effective reflectance of each target for each imaging band of the WVMI is calculated as follows:

$$R_e = \frac{\int_{\lambda_1}^{\lambda_2} R_\lambda S_\lambda \, d\lambda}{\int_{\lambda_1}^{\lambda_2} S_\lambda \, d\lambda}, \tag{4}$$

where λ_1 and λ_2 are the minimum and maximum wavelengths of each imager band, S_λ is the spectral response at wavelength λ and R_λ is the reflectance of the target at wavelength λ. This effective reflectance serves as input to the radiative transfer model and new apparent radiances are calculated. These are compared to the apparent radiances obtained from Equation (3). Differences reflect how well the calibration was performed; the results are summarized in Table 1.

6. Discussion

For the imager's green and red bands, errors between radiative transfer calculations and calculations using the calibration equation for the CHY target with relatively high and stable reflectance in these two bands, are the lowest: 1.7% for the green band and 1.6%

Table 1. Errors between radiative transfer calculations and calibration calculations using Equation (3) for the four validation targets.

Target	Calculated radiance of the green band ($W\ m^{-2}\ sr^{-1}\ \mu m^{-1}$)	Calibrated radiance of the green band ($W\ m^{-2}\ sr^{-1}\ \mu m^{-1}$)	Relative error (%)	Calculated radiance of the red band ($W\ m^{-2}\ sr^{-1}\ \mu m^{-1}$)	Calibrated radiance of the red band ($W\ m^{-2}\ sr^{-1}\ \mu m^{-1}$)	Relative error (%)	Calculated radiance of the infrared band ($W\ m^{-2}\ sr^{-1}\ \mu m^{-1}$)	Calibrated radiance of the infrared band ($W\ m^{-2}\ sr^{-1}\ \mu m^{-1}$)	Relative error (%)
CHR	43.45	39.31	9.6	127.80	130.08	1.8	103.17	106.66	3.4
CHY	153.59	156.22	1.7	159.27	161.85	1.6	110.50	111.42	0.8
CHG	33.52	40.31	20.2	14.10	15.80	12.1	20.17	20.19	0.1
CHB	62.89	64.02	1.8	35.86	34.33	4.2	79.32	67.87	14.4

for the red band. For the CHB and CHR targets, the reflectances of which are smaller than those of the CHY target and exhibit significant variations, the errors are slightly larger but generally less than 5.0%, except for the case of the CHR target in the green band (9.6%). Errors for the CHG target, the reflectance of which can reach as low as 5.0%, are the largest: 20.2% for the green band and 12.1% for the red band. This shows that for green and red bands, large uncertainties will occur when using the calibration equation to retrieve surface parameters over a surface with a low reflectance, such as over a vegetated land surface. In the infrared band, errors for the CHY, CHR, and CHG targets are less than 5.0% and for the CHB target, the error reaches a maximum of 14.4%.

In general, for those targets with a high reflectance and a stable spectrum, the use of the calibration equation will result in smaller errors. Using the calibration equation for targets with low reflectance that vary noticeably with wavelength will increase uncertainties in retrievals. As for a sensor like the WVMI with a spectral resolution of 0.1 μm, sharp increases or decreases in reflectance will result in errors when assessing the contribution from different wavelengths because the solar spectrum is not smooth and varies with wavelength. However, a low reflectance means that the contribution of the surface is relatively low and that the scattering of the atmosphere is important and should not be neglected. Because gains and biases are derived through the least-squares method, the absolute error for low reflectance is small. Compared to the small amount of total energy that the sensor receives, tiny absolute errors morph into large relative errors. For the imager's green and red bands, targets with lower reflectance will generate larger errors than those with a larger reflectance, which varies with wavelength in a similar manner, indicating that for these bands, atmospheric molecular and aerosol scatterings are strong and have a more important contribution to the total energy the sensor receives. In the infrared band, where atmospheric molecular scattering and aerosol scattering are weaker, sharp variations in reflectance will contribute more to the total energy the sensor receives because they alter the energy distribution at different wavelengths.

7. Summary and conclusions

The in-flight absolute radiometric calibration of the WVMI in an unmanned vehicle was performed using a reflectance-based method. In order to get proper calibration equations (mainly gains and biases), we designed and deployed a set of six radiometric calibration targets with flat spectra. The least-squares method was used for generating gains and biases with the least error. Calibration results show that linear correlations between sensor output and apparent radiances received by the sensor are very high, with an r^2 value of up to 0.99 for each band. In order to validate the calibration result and estimate the spectrum unevenness common in nature, we deployed a set of four radiometric validation targets with different uneven reflectance spectra. Through the generation of effective reflectances in each band at each target, we calculated apparent radiances using a radiative transfer model and then compared them to those calculated using the calibration equation. The results reveal that errors are very low (less than 2.0%) for those targets with high reflectance that varies less with wavelength. For targets with low reflectance or reflectances that vary noticeably with wavelength, errors are relatively large and depend on the band. A further analysis shows that large errors (up to 10.0–20.0%) occur in these green and red bands when reflectances are of the order of 5.0–10.0%. This may affect any application involved with very low surface reflectances at these two bands.

Acknowledgement

This research is funded by the China Scholarship Council and a 863 project of UAV Sensor Calibration Test under contract 2008AA121806.

References

Biggar, S. F., M. C. Dinguirard, G. I. Gellman, P. Henry, R. D. Jackson, M. S. Moran, and P. N. Slater. 1991. "Radiometric Calibration of SPOT 2 HRV-a Comparison of Three Methods." *Proceeding SPIE* 1493: 155–62.

Biggar, S. F., R. P. Santer, and P. N. Slater. 1990. "Irradiance-Based Calibration of Imaging Sensors." In *The Proceedings of the IEEE International Geoscience and Remote Sensing Symposium*. College Park, MD, vol. 1, 507–10.

Biggar, S. F., P. N. Slater, and D. I. Gellman. 1994. "Uncertainties in the in-Flight Calibration of Sensors with Reference to Measured Ground Sites in the 0.4–1.1 um Range." *Remote Sensing of Environment* 48: 245–52.

Biggar, S. F., K. J. Thome, and W. Wisniewski. 2003. "Vicarious Radiometric Calibration of EO-1 Sensors by Reference to High-Reflectance Ground Targets." *IEEE Transactions on Geoscience and Remote Sensing* 41: 1174–9.

Cihlar, J., J. Chen, and Z. Li. 1997. "Seasonal AVHRR Multichannel Data Sets and Products for Studies of Surface-Atmosphere Interactions." *Journal of Geophysical Research* 102: 625–9, 640.

Gao, H., X. Gu, T. Yu, H. Gong, J. Li, and X. Li. 2010. "HJ-1A HSI on-Orbit Radiometric Calibration and Validation Research." *Science China-Technological Sciences* 53: 3119–28.

Lee, K., Z. Li, Y. J. Kim, and A. Kokhanovsky. 2009. "Atmospheric Aerosol Monitoring From Satellite Observations: A History of Three Decades." In *Atmospheric and Biological Environmental Monitoring*, edited by Y. J. Kim, U. Platt, M. B. Gu, and H. Iwahashi, 13–38. Berlin: Springer.

Li, Z., X. Zhao, R. Kahn, M. Mishchenko, L. Remer, K.-H. Lee, M. Wang, I. Laszlo, T. Nakajima, and H. Maring. 2009. "Uncertainties in Satellite Remote Sensing of Aerosols and Impact on Monitoring its Long-term Trend: A Review and Perspective." *Annales Geophysicae* 27: 1–16.

Naughton, D., A. Brunn, J. S. Czapla-Myers, S. Douglass, M. Thiele, H. Weichelt, and M. Oxfort. 2011. "Absolute Radiometric Calibration of the RapidEye Multispectral Imager Using the Reflectance-Based Vicarious Calibration Method." *Journal of Applied Remote Sensing* 5: 053544. doi:10.1117/1.3613950.

Rondeaux, G., M. D. Steven, J. A. Clark, and G. Mackay. 1998. "La Crau: A European Test Site for Remote Sensing Validation." *International Journal of Remote Sensing* 19: 2775–88.

Slater, P. N., S. F. Biggar, R. G. Holm, R. D. Jackson, Y. Mao, M. S. Moran, J. M. Palmer, and B. Yuan. 1987. "Reflectance- and Radiance-Based Methods for the in-Flight Absolute Calibration of Multispectral Sensors." *Remote Sensing of Environment* 22: 11–37.

Thome, K. J. 2001. "Absolute Radiometric Calibration of Landsat 7 ETM+ Using the Reflectance-Based Method." *Remote Sensing of Environment* 78: 27–38.

Thome, K. J. 2005. "Sampling and Uncertainty Issues in Trending Reflectance-Based Vicarious Calibration Results." *SPIE* 5882: 1–10.

Thome, K. J., D. L. Helder, D. Aaron, and J. D. Dewald. 2004. "Landsat-5 TM and Landsat-7 ETM+ Absolute Radiometric Calibration Using the Reflectance-Based Method." *IEEE Transactions on Geoscience and Remote Sensing* 42: 2777–85.

Xiong, X. X., and W. Barnes. 2006. "An Overview of MODIS Radiometric Calibration and Characterization." *Advances in Atmospheric Sciences* 23: 69–79.

Zhang, Y., X. F. Gu, T. Yu, Y. Zhang, L. Chen, X. Li, X. Li, and L. He. 2005. "Absolute Radiometric Calibration of CBERS-02 IRMSS Thermal Band." *Science in China Series E-Engineering & Materials Science* 48: 72–90.